NJC

Accepted Manuscript

This is an *Accepted Manuscript*, which has been through the RSC Publishing peer review process and has been accepted for publication.

Accepted Manuscripts are published online shortly after acceptance, which is prior to technical editing, formatting and proof reading. This free service from RSC Publishing allows authors to make their results available to the community, in citable form, before publication of the edited article. This *Accepted Manuscript* will be replaced by the edited and formatted *Advance Article* as soon as this is available.

To cite this manuscript please use its permanent Digital Object Identifier (DOI®), which is identical for all formats of publication.

More information about *Accepted Manuscripts* can be found in the **Information for Authors**.

Please note that technical editing may introduce minor changes to the text and/or graphics contained in the manuscript submitted by the author(s) which may alter content, and that the standard **Terms & Conditions** and the **ethical guidelines** that apply to the journal are still applicable. In no event shall the RSC be held responsible for any errors or omissions in these *Accepted Manuscript* manuscripts or any consequences arising from the use of any information contained in them.

New Journal of Chemistry

Dynamic Article Links ►

Cite this: DOI: 10.1039/c0xx00000x

www.rsc.org/xxxxxx

PAPER

Ultralong $H_2V_3O_8$ Nanowire Bundles as a Promising Cathode for Lithium Batteries†

Qinyou An,[a] Jinzhi Sheng,[a] Xu Xu,[a] Qiulong Wei,[a] Yaqin Zhu,[b] Chunhua Han,*[a] Chaojiang Niu[a] and Liqiang Mai*[a]

Received (in XXX, XXX) Xth XXXXXXXXX 20XX, Accepted Xth XXXXXXXXX 20XX
DOI: 10.1039/b000000x

Ultralong $H_2V_3O_8$ nanowire bundles with length up to hundreds of micrometers are successfully synthesized by a facile hydrothermal approach. The nanowire bundles exhibits a high specific discharge capacity of 325.7 mAh/g at 50 mA/g. While the current density is up to 2000 mA/g, the initial specific discharge capacities of $H_2V_3O_8$ nanowires cathode can reach to 121.1 mAh/g with a capacity fading of only 0.0425% per cycle for 300 cycles. Electrical transport of the single nanowire was also recorded *in situ* to detect the evolution of the nanowire during annealing. The conductivity of $H_2V_3O_8$ nanowires has an increase of three orders of magnitudes compared to that of the dehydrated nanowires. The excellent electrochemical performances of $H_2V_3O_8$ nanowire bundles result from high conductivity and good structural stability. This work demonstrates that $H_2V_3O_8$ nanowire bundle is a promising cathode material for lithium batteries.

Introduction

With the rapid depletion of world oil reserves, constantly emergence of their related hazards, and wide applications from advanced portable electronic devices to electric vehicles (EVs) and smart grids, the demand for lithium storage device with high energy and power densities is increasing continuously.[1-5] Indeed, lithium batteries have achieved a leading role in the consumer electronics market with further improvements in terms of energy and power densities. However, there are still required for making this systems suitable for application in electric vehicle sector[4-6] In order to increase the high-rate capability and cycle life, many efforts have been done, such as the introduction of electronically conductive phases or the fabrication of unique nanoarchitectures.[6-10] Due to the high electrode-electrolyte contact area, fast Li^+ diffusion and good strain release, one-dimensional nanomaterials have raised great attentions in lithium batteries.[9,11]

Vanadium oxides are among the best cathode materials for rechargeable lithium batteries, due to both their large specific capacity and abundant sources.[12-15] However, the development of many vanadium oxides electrodes in lithium batteries has been limited by its poor structural stability, low electronic conductivity and slow electrochemical kinetics.[16-18] In particular, $H_2V_3O_8$ is an intermediate phase in which the ratio of V^{4+}/V^{5+} is 1/2, which would account for a larger theoretical capacity and better resistance to oxidation in air than the metastable VO_2.[19] Compared to V_2O_5, $H_2V_3O_8$ has a higher electronic conductivity arising from a mixed-valence of V^{4+}/V^{5+}.[19,20] In recent years, one-dimensional $H_2V_3O_8$ nanostructures have been successfully fabricated by a variety of methods and the electrochemical kinetics is indeed improved.[20-23] Nevertheless, it still remains as a big challenge to obtain a long-term cycling stability during subsequent rapid lithium insertion/extraction processes.[24] Here, we reported a facile hydrothermal method to synthesize $H_2V_3O_8$ nanowires, and the electrical transport property of the single nanowire was tested. The $H_2V_3O_8$ nanowires cathode showed excellent high rate performance and good cycle stability.

Experimental Section

Sample preparation

The synthesis route of ultralong $H_2V_3O_8$ nanowire bundles was modified from our previous works.[24] Basically, vanadium oxide nanowires were successfully prepared by hydrothermal reaction using V_2O_5 sol. Briefly, 1.3 mmol of the as-prepared V_2O_5 sol, 3.6 μL of aniline, and 0.04 g of poly(ethylene glycol) (PEG-4000) were mixed by stirring and then transferred into a Telfon-lined stainless steel autoclave and kept at 180 °C for 2 days. The products were collected and washed repeatedly with deionized water and ethanol, and finally dried at 80 °C for 12 h in air to obtain the ultralong $H_2V_3O_8$ nanowire bundles. In addition, the resultant $H_2V_3O_8$ nanowire bundles was annealed at 400 °C for 3 h in N_2 to obtain V_3O_7 nanowire as a control sample.

Material characterization

An X-ray diffraction (XRD) measurement was performed to investigate the crystallographic information using a D/MAX-III X-ray diffractometer with graphite-monochromatized Cu Kα radiation. Thermogravimetry/differential scanning calorimetry (TG/DSC) was performed using a Netzsch STA 449C simultaneous thermal analyzer at a heating rate of 10 °C/min in

N_2. Field emission scanning electron microscopy (FESEM) images were collected with a Hitachi S-4800. Transmission electron microscopy (TEM), high-resolution transmission electronmicroscopy (HRTEM) images were recorded by using a JEM-2100F microscope.

Electrochemical measurements

Electrodes were fabricated using a mixture of the nanowires, acetylene black, and PTFE (polytetrafluoroethylene) in a 70:20:10 weight ratio as the cathode. The thickness of both the electrodes was 30 μm. The electrochemical properties of the electrodes were measured using R2025 coin-type cells in a glove box filled with pure argon gas, which using lithium pellet as the anode, 1 M solution of $LiPF_6$ in ethylene carbon (EC)/dimethyl carbonate (DMC) as electrolyte. Galvanostatic measurements of the cells were carried out over the potential region of 1.50 - 3.75 V with a multichannel battery testing system (LAND) at room temperature. Cyclic-voltammetry (CV) and electrochemical impedance spectroscopy of the cells were carried out using an electrochemical analyzer (Autolab PGSTAT 302 and CHI 760D potentiostat/galvanostat). In impedance measurements, the frequency range of 100 kHz to 0.01Hz was used.

Results and Discussion

The products were initially characterized by X-ray diffraction (XRD) patterns to identify the crystallographic structure and crystallinity. The XRD pattern of $H_2V_3O_8$ (**Figure 1a**) shows the formation of orthorhombic structure (JCPDS NO. 01-085-2401). The sharp diffraction peaks imply that the obtained $H_2V_3O_8$ nanowire is well crystallized. The sintered V_3O_7 is a monoclinic structure (**Figure S1**). It indicates that the

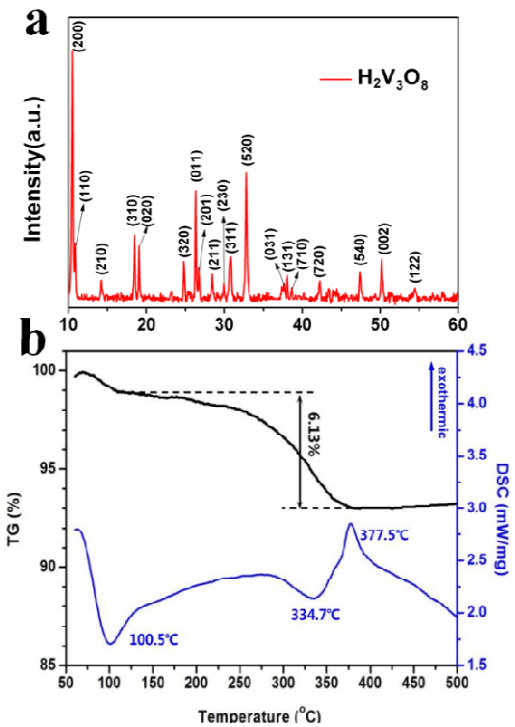

Figure 1. (a) XRD patterns of $H_2V_3O_8$ nanowires. (b) Thermogravimetric analysis of $H_2V_3O_8$ in N_2.

phase structure rebuilt from orthorhombic to monoclinic during the annealing process. In order to confirm the phase transition, thermogravimetric analysis of the $H_2V_3O_8$ nanowire bundles was carried out in a flowing N_2 atmosphere (**Figure 1b**). The TG curve shows two steps whichare related to dehydration. The first step up to 125 °C is attributed to the removal of absorbed water on the surface of the product, which can be confirmed by the endothermic peak of the DSC curve. The second step up to 377.5 °C exhibits the loss of water in the crystal structure, which is corresponding well to the endothermic DSC peak at ~350 °C. The weight lose in this step is 6.1%, and the value is close to the theoretical weight of the structural water (6.4%) in $H_2V_3O_8$.[25] There is no weight change from 377.5 °C to 500 °C, which indicates that the water is released completely. While it appears an exothermic peak which is rarely seen in the past reports, it is confirmed that there is a phase transformastion of V_3O_7 to form a more stable structure. There is no obvious boundary between the second endothermic and exothermic peaks, indicating the structure rebuilt is along with the dehydration process.

The structure of $H_2V_3O_8$ is a nearly two-dimensional framework (V_3O_8 layer) comprised of VO_6 octahedra and VO_5 trigonal bipyramid.[26,27] It is very difficult to determine the positions of hydrogen directly, but according to reported results, there is one or two hydrogen atoms firmly attached to VO_6 octahedron and making hydrogen bonds with the octahedral in the next layer to hold the V_3O_8 layers giving the three-dimensional structure.[28] When two hydrogen atoms attach, it is thought that the water molecule shares one oxygen atom with VO_6.[20, 29] While the unit cell of V_3O_7 is composed of twelve VO_6 octahedras, sixteen VO_5 trigonal bipyramids and eight VO_5 square pyramids, the V_3O_7 is no longer a layer structure.[30]

The morphology and microstructure of the products were investigated by field emission scanning electron microscopy (FESEM) and transmission electron microscope (TEM). The FESEM images (**Figure 2a, b**) reveal that the $H_2V_3O_8$ product is composed of uniform nanowires with a diameter of ~100 nm and a length of several hundred micrometers. Further, many nanowires are almost arranged along the same direction, and forming $H_2V_3O_8$ nanowire bundles. After annealing at 400 °C in N_2, the bundled structure still remains (**Figure S2a, b**). According to the HRTEM (**Figure 2c**), the lattice fringes of $H_2V_3O_8$ nanowire with regular spacing, the well-resolved fringes confirm the single-crystal nature of the $H_2V_3O_8$ nanowires, which is in accordance with the selected area electron diffraction (SAED) patterns, while the lattice fringes of V_3O_7 nanowire is not so clear with lattice defect in the HRTEM image (**Figure S2c**).

The long chain linear polymer molecules were widely used as template in synthesizing ultralong nanowires.[31] The polymer template polyethylene glycol (PEG) is reported to play an important role in forming monodirection ultralong nanowires.[32] Ratio-dependent (V_2O_5 sol to PEG) experiments were performed to gain insight into the formation process of such uniform $H_2V_3O_8$ nanowires. Products were collected at different ratio from 4:0 to 4:2, and their morphologies were subjected (**Figure S3**). When the absence of PEG, the nanowires are only less than ten micrometers with nonhomogeneous diameter, and lay in the random direction. With the increase of PEG, the nanowires

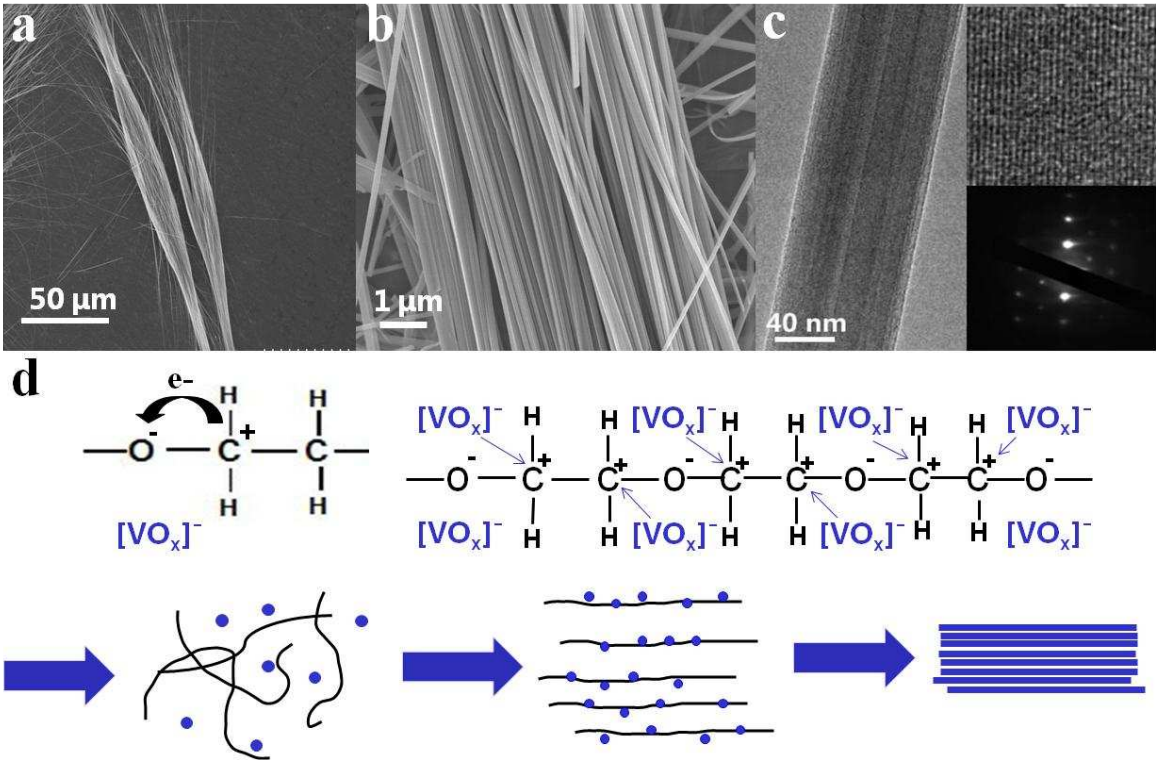

Figure 2. (a, b) SEM images of the bunched $H_2V_3O_8$ nanowires. (c) TEM images and SAED pattern (down inset) of $H_2V_3O_8$ nanowires. (d) The schematic illustration of the formation of bunched $H_2V_3O_8$ nanowires.

become dozens of micrometers long, and also exhibit a bunched morphology. It indicates that PEG is necessary for the quasi-monodirectional structure. In addition, the V_2O_5 powder was also used instead of the sol with PEG (**Figure S4**). The length of the obtained nanowires is also up to dozens of micrometers, but the nanowires arrange in random directions. According to these results, we conclude the following growth mechanism in **Figure 2d**. Firstly, it is well know that inductive effects universally exist in most polymers, and according to the electronegativity theory, the electron clouds will shift to the oxygen atoms in PEG[28]. So the polyoxovanadate clusters with negative charge in V_2O_5 sol[33] were covered on the linear PEG by electrostatic effect with $C^{\delta+}$. Secondly, the reduction of V_2O_5 was caused by both aniline and PEG, meanwhile the aniline transformed into polyaniline[43] and the PEG were oxidized[40,41,43,44]. The EDS spectra in **Figure S6** shows that there is no nitrogen in the nanowires, which proves that polyaniline did not exist in the nanowires, and it may be decomposed during the hydrothermal process. Also the EDS spectra (**Figure S6**) displays the existence of carbon in the $H_2V_3O_8$ nanowires, indicating that there are some organics remained in the nanowires, which should derive from the oxidation of PEG, and two absorption peaks at 1390 cm^{-1} and 1585 cm^{-1} in the FT-IR spectra (**Figure S7**) support the presence of —COOH. Thus the redox process can be described as follows[40].

$$12V_2O_5 + —CH_2CH_2OCH_2CH_2O— \rightarrow$$
$$8V_3O_7 + —CH_2COOH + —OCH_2COOH + H_2O$$

Thirdly, it is well known that the same charge would repel each other[41,42], so the polyoxovanadate clusters repel each other, and gradually be parallel each other to reduce the systemic energy. Finally, the ultralong $H_2V_3O_8$ nanowire bundles were synthesized.

Coin cells with metallic lithium as an anode were assembled to investigate the electrochemical performance of the ultralong $H_2V_3O_8$ nanowires cathodes. Cyclic voltammogram (CV) curves of the $H_2V_3O_8$ and V_3O_7 nanowires was measured at a scan rate of 0.1 mV/s in the potential range from 1.5 to 3.75 V (**Figure 3a**). The cathodic and anodic peaks are ascribed to the lithium ion

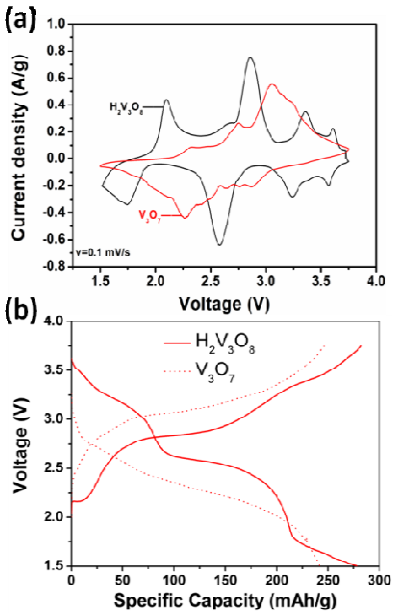

Figure 3. (a) Cyclic voltammogram curves of $H_2V_3O_8$ and V_3O_7 nanowires electrodes at scanning rate of 0.1 mv/s. (b) Charge-discharge curves of $H_2V_3O_8$ and V_3O_7 nanowires electrodes at different cycles under

100 mA/g.

insertion and extraction, respectively. For $H_2V_3O_8$ nanowires, the four pairs well defined redox peaks appear at 2.10/1.74 V, 2.86/2.58 V, 3.36/3.24 V and 3.61/3.57 V, while the main redox peak of V_3O_7 nanowire electrode is observed at 3.06/2.33 V. The charge–discharge voltage profiles of the $H_2V_3O_8$ and V_3O_7 nanowires electrodes at the first cycle are shown in **Figure 3b**. It is evident that four plateaus are displayed in the discharge process of the $H_2V_3O_8$ nanowires cathode, while there is only one main plateau in the discharge process of V_3O_7 nanowires cathode, which agrees well with CV results.

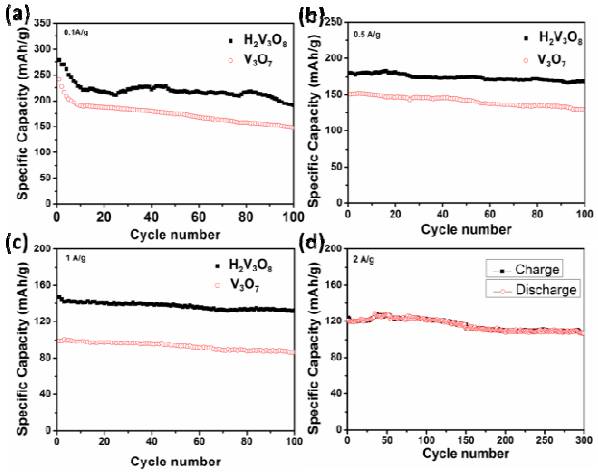

Figure 4. The cycling performance of $H_2V_3O_8$ and V_3O_7 nanowires electrodes at the current densities of (a) 100 mA/g, (b) 500 mA/g, (c) 1000 mA/g. (d) Cycling performance of the $H_2V_3O_8$ nanowires electrode at the current density of 2000 mA/g.

The cycling stability of the $H_2V_3O_8$ and V_3O_7 nanowires at different current densities of 100 - 1000 mA/g are shown in **Figure 4**. The initial discharge capacity of $H_2V_3O_8$ and V_3O_7 deliver 278.1 mAh/g and 241.8 mAh/g at the current density of 100 mA/g, respectively. The capacity of the $H_2V_3O_8$ nanowires slightly decayed to ~226 mAh/g in the tenth cycle, and became relatively stable in the further cycles. This stabilized capacity of $H_2V_3O_8$ nanowires is significantly higher than that of V_3O_7 nanowires. While at the current densities of 500 and 1000 mA/g, the discharge capacity only suffered a slightly decrease. For example, after 100 cycles, the discharge capacities of $H_2V_3O_8$ and V_3O_7 were found to be 167.8 mAh/g (93.1% of the initial capacity) and 128.5 mAh/g (85.2% of the initial capacity) at the current density of 500 mA/g, respectively. The long-life cycling performance of the $H_2V_3O_8$ nanowires at the high rate is also shown in **Figure 5d**. Stable cycling performance is obtained for the rate. After 300 cycles at 2000 mA/g, 88.0% of the initial capacity (~120 mAh/g) can be retained, corresponding to the capacity fading of 0.0425% per cycle. However, V_3O_7 nanowires electrode delivers only an intial discharge capacity of 86.6 mAh/g (**Figure S5**). It can be obviously found that the $H_2V_3O_8$ nanowires exhibited the higher capacity and better cycling performance than V_3O_7 nanowires at different current densities, especially at high current densities.

To evaluate the rate capability, $H_2V_3O_8$ nanowires were cycled at a various charge/discharge rates ranging from 50 to 2000 mA/g (**Figure 5a**). The initial discharge capacity of $H_2V_3O_8$ nanowires can reach as high as 325.7 mAh/g at the current density of 50 mA/g, the inserted Li^+ amount (x in $Li_xH_2V_3O_8$) achieves 3.44, the values is much higher than the reported results.[22, 27, 29] As the current density increases from 100 to 200, 300, 500, 1000, 2000 mA/g, the discharge capacity decreases gradually from 285.1 to 248.8, 221.8, 197.4, 136.4 and 102.6 mAh/g, respectively. After the high rate measurement, the current density is reduced back to 100 mA/g, and a discharge capacity of ~245 mAh/g can be recovered. It can be seen that the $H_2V_3O_8$ nanowires show higher capacity and better rate capabilities than V_3O_7 nanowires. The electrochemical performances of the ultralong $H_2V_3O_8$ NWs are comparable to those of many reported $H_2V_3O_8$ electrodes[19,20,22] (Table S1).

As we know, the power capability of an insertion electrode material depends on the kinetics of the lithium ion extraction/insertion process which is related to the electron transport and lithium ion diffusion length.[34,35] As the rate capability is directly related to the impedance of a cell, the electrochemical impedance spectroscopy (EIS) of $H_2V_3O_8$ and V_3O_7 nanowires electrodes were also measured to provide further insights. The Nyquist plots for $V_3O_7{\cdot}H_2O$ and V_3O_7 nanowires electrodes show a straight line in the low frequency region and a depressed semicircle in the high frequency region (**Figure 5b**). The size of the semicircle, which measures the charge transfer impedance in the electrode,[36] was clearly smaller for the $H_2V_3O_8$ nanowires electrode. The better connectivity and layered structure of the bundled $H_2V_3O_8$ nanowires may be the main reason of the reduced charge-transfer resistance.

To understand the superior performance of $H_2V_3O_8$ nanowires for Li^+ storage, we measured the electrical transport through single nanowire transport properties before and after annealing (Figure 5c-e). We deposit vanadium oxide nanowires on the silicon wafer followed by current collector patterning with e-beam lithography and deposition of Cr/Au (10/100 nm) with thermal evaporator. Before annealing, the *I–V* characteristics of the nanowire showed ohmic behavior (Figure 5d), and the transported current was in the order of ca. 10 μA at 4 V. After annealing, the *I–V* curve showed asymmetric Schottky barriers (Figure 5e), and the transported current was of the order of 3 nA at ca. 4 V. Therefore, the conductivity of $H_2V_3O_8$ nanowire increased by close to three orders of magnitudes compared to that of the dehydrated nanowire, which indicates the conversion of $H_2V_3O_8$ nanowire from metallic to semiconductor behaviour during the heat treatment.

The excellent electrochemical performance of ultralong $H_2V_3O_8$ nanowire bundles, especially at high rate charge and discharge, may be attributed to: (1) the ultralong nanowires provide short distances for Li ions diffusion and large electrode–electrolyte contact area for rapid Li ions transport across the interface, leading to a better rate capability;[9, 10, 37, 38] (2) The ultralong structured nanowires not only provide long continuous channel for electrons to transport, but also efficiently reduce the aggregation of the materials.[11] Consequently, it keeps their high active surface area, which is favorable for increasing the lithium storage capacity in the electrode; (3) The $H_2V_3O_8$ has a higher electronic conductivity arising from a mixed-valence of V^{4+}/V^{5+};[21, 29] (4) The hydrogen linked the V_3O_8 layers provide an

elastic buffer space to accommodate the volume expansion/contraction of vanadium layers during Li insertion/extraction process, thus maintaining the high capacity and good cycling stability.[39]

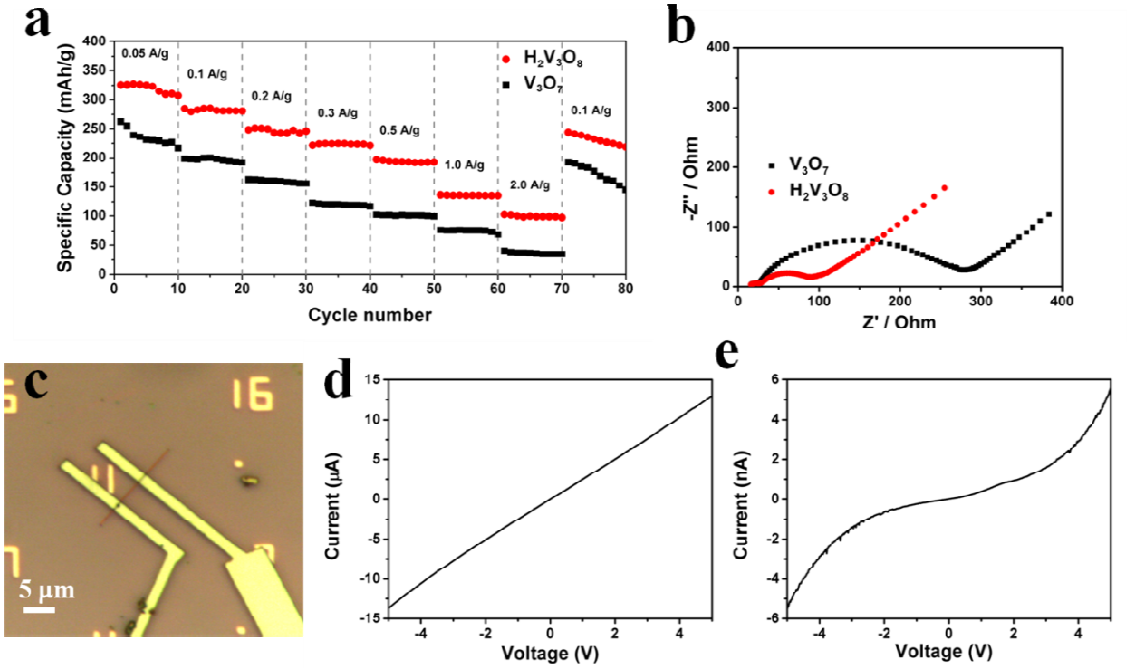

Figure 5. (a) Rate performances of $H_2V_3O_8$ and V_3O_7 nanowires electrodes. (b) Nyquist plots of $H_2V_3O_8$ and V_3O_7 nanowires electrodes in newly assembled cells. (c) The SEM image of single nanowire device. Single nanowire transport properties of (d) $H_2V_3O_8$ and (e) V_3O_7 nanowires.

Conclusions

Ultralong $H_2V_3O_8$ nanowire bundles have been successfully synthesized, which deliver high specific reversible capacity (325.7 mAh/g) and excellent cycling stability (over 88% capacity retention after 300 cycles at 2000 mA/g). Compared to V_3O_7 nanowire bundles, ultralong $H_2V_3O_8$ nanowire bundles also exhibit better rate capability. The excellent electrochemical performance of the ultralong $H_2V_3O_8$ nanowire bundles cathode indicates its potential application in high-rate and long-life secondary lithium batteries. The synthesis strategy demonstrated is facile and versatile for the fabrication of other cathode materials.

Acknowledgements

This work was supported by the National Basic Research Program of China (2013CB934103, 2012CB933003), the National Natural Science Foundation of China (51072153, 51272197), the Program for New Century Excellent Talents in University (NCET-10-0661) and the Fundamental Research Funds for the Central Universities (2013-VII-028). Thanks to Prof. C.M. Lieber of Harvard University, Prof. Dongyuan Zhao of Fundan University and Dr. Jun Liu of Pacific Northwest National Laboratory for strong support and stimulating discussion.

Notes and references

[a] *WUT-Harvard Joint Nano Key Laboratory, State Key Laboratory of Advanced Technology for Materials Synthesis and Processing, Wuhan University of Technology, Wuhan, 430070, P. R. China. Fax: +86-027-87644867; Tel: +86-027-87467595; E-mail: mlq518@whut.edu.cn; hch5927@whut.edu.cn*

[b] *Shanghai Institute of Ceramics, Chinese Academy of Sciences, Shanghai, 2000 50, P. R. China.*

† Electronic Supplementary Information (ESI) available: XRD of V_3O_7 nanowires; SEM and TEM images of the V_3O_7 nanowires; the SEM images of the products prepared in different mass ratio (V_2O_5 sol to PEG) from 4:0 to 4:2; the SEM image of the product prepared by the V_2O_5 powder; Cycle stability of the V_3O_7 nanowires electrode at the current density of 2000 mA/g. See DOI: 10.1039/b000000x/

1 B. Kang and G. Ceder, *Nature*, 2009, **458**, 190.
2 J. M. Tarascon and M. Armand, *Nature*, 2001, **414**, 359.
3 P. Simon and Y. Gogotsi, *Nat. Mater.*, 2008, **7**, 845.
4 C. Liu, F. Li, L. P. Ma and H. M. Cheng, *Adv. Mater.*, 2010, **22**, E28.
5 P. G. Bruce, B. Scrosati and J. M. Tarascon, *Angew. Chem. Int. Ed.*, 2008, **47**, 2930 .
6 J. Yan, A. Sumboja, E. Khoo and P. S. Lee, *Adv. Mater.*, 2011, **23**, 746.
7 R. Krishnan, T. Ming. Lu and N. Koratkar, *Nano Lett.*, 2011, **11**, 377.
8 H. Zhang, X. D. Yu and P. V. Braun, *Nat. Nanotechnol.*, 2011, **6**, 277.
9 C. K. Chan, H. Peng, G. Liu, K. Mcilwrath, X. F. Zhang, R. A. Huggins and Y. Cui, *Nat. Nanotechnol.*, 2008, **3**, 31.
10 J. Liu, H. Xia, D. F. Xue and L. Lu. *J. Am. Chem. Soc.*, 2009, **131**, 12086.
11 L. Q. Mai, L. Xu, C. H. Han, X. Xu, L. Z. Luo, S. Y. Zhao and Y. L. Zhao, *Nano Lett.*, 2010, **10**, 4750.
12 V. Legagneur, A. Le Gal La Salle, A. Verbaere, Y. Piffard and D. Guyomard, *Electrochim. Acta*, 2002, **47**, 1153.
13 M. S Whittingham, Y. N. Song, S.Lutta, P. Y. Zavalij and N. A. Chernova, *J. Mater. Chem.*, 2005, **15**, 3362.
14 H. C. Pang, P. Cheng, H. B. Yang, J. L. Lu, C. X. Guo, G. L. Ning and C. M. Li, *Chem. Commun.*, 2013, **49**, 1536.
15 A. Pan, ZJ. G. hang, Z. Nie, G. Cao, B. W. Arey, G. Li, S. Q. Liang

and J. Liu, *J. Mater. Chem.*, 2010, **20**, 9193.
16 C. Ban, N. A. Chernova and M. S. Whittingham, *Electrochem. Commun.*, 2009, **11**, 522.
17 J. Muster, G. T. Kim, V. Krstić, J. G. Park, Y. W. Park, S. Roth and M. Burghard, *Adv. Mate.*, 2000, **12**, 420.
18 T. Watanabe, Y. Ikeda, T. Ono, M. Hibino, M. Hosoda, K. Sakai and T. Kudo, *Solid State Ionics*, 2002, **151**, 313.
19 H. Q. Li, T. Y. Zhai, P. He, Y. G. Wang, E. Hosonoa and H. S. Zhou, *J. Mater. Chem.*, 2011, **21**, 1780.
20 S. K. Gao, Z. J. Chen, M. D. Wei, K. M. Wei and H. S. Zhou, *Electrochim. Acta*, 2009**, 54***,* 1115.
21 C. Tsang and A. Manthiram, *J. Electrochem. Soc.*, 1997, **144**, 520.
22 H. Qiao, X. J. Zhu, Z. Zheng, L. Liu and L. Zhang, *Electrochem. Commun.*, 2006, **8**, 21.
23 P. G. Jesús, M. S. Beatriz, A. B. David, M. Emilio, P. F. Juan Carlos, K. Alois and G. A. Flaviano. *J. Power Sources*, 2013**, 232**, 173.
24 L. Q. Mai, Y. J. Dong, L. Xu and C. H. Han, *Nano Lett.*, 2010, **10**, 4273.
25 J. Wang, C. J. Curtis, D. L. Schulz and J. G. Zhang, *J. Electrochem. Soc.*, 2004, **151**, A1.
26 Y. Oka, T. Yao and N. Yamamoto, *J. Solid State Chem.*, 1990, **89**,372.
27 T. Chirayil, P. Y. Zavalij and M. S. Whittingham, *Chem. Mater.*, 1998, **10**, 2629.
28 N. E. Sladek and G. J. *Molecular pharmacology*, 1969, **5**: 174.
29 Y. Wang and G. Z. Cao, *Chem. Mater.*, 2006, **18**, 2787.
30 C. Li, M. Isobe, H. Ueda, Y. Matsushita and Y. Ueda, *J. Solid State Chem.*, 2009, **182**, 3222.
31 C.V. Subba Reddya, S. Mhoa, R. R. Kalluru and Q. L. Williams, *J. Power Sources*, 2008, **179**, 854.
32 X. Xu, Y. Z. Luo, L. Q. Mai, Y. L. Zhao, Q. Y. An, L. Xu, F. Hu, L. Zhang and Q. J. Zhang, *NPG Asia Mater.*, 2012**, 4**, e20.
33 J. Livage, *Chem. Mater.*, 1991, **3**, 578.
34 H. G. Jung, S.-T. Myung, C. S. Yoon, S.-B. Son, K. H. Oh, K. Amine, B. Scrosati and Y.-K. Sun, *Energy Environ. Sci.*, 2011, **4**, 1345.
35 J. Liu, T. E. Conry, X. Y. Song, M. M. Doeff and T. J. Richardson, *Energy Environ. Sci.*, 2011, **4**, 885.
36 R. Ruffo, S. S. Hong, C. K. Chan, R. A. Huggins and Y. Cui, *J. Phys. Chem. C*, 2009, **113**, 11390.
37 T. Y. Zhai, H. M. Liu, H. Q. Li, X. S. Fang, M. Y. Liao, L. Li, H. S. Zhou, Y. Koide, Y. Bando and D. Golberg, *Adv. Mater.*, 2010, **22**, 2547.
38 L. Zhou, D. Y. Zhao and X. W. Lou, *Angew. Chem. Int. Ed.*, 2012, **51**, 239
39 M. D. Wei, H. Sugihara and I. Honma, *Adv. Mater.*, 2005, **17**, 2964.
40 D. Mantzavinos, E. Lauer, M. Sahibzada, A. Livingston and I. Metcalfe. *Water Research*, 2000, **34**: 1620.
41 Z. Kang, E. Wang, M. Jiang, S. Lian, Y. Li, C. Hu, *European Journal of Inorganic Chemistry*, 2003, **2003**, 370.
42 H. Daiguji, P. Yang and A. Majumdar, *Nano Letters*, 2004, **4**, 137.
43 L. Q. Mai, X. Xu, C. H. Han, Y. Z. Luo, L. Xu, Y. M. Wu, Y. L. Zhao, *Nano letters*, 2011, **11**, 4992.
44 L. Q. Mai, Q. L. Wei, Q. Y. An, X. C. Tian, Y. L. Zhao, X. Xu, L. Xu, L. Chang, Q. J. Zhang, *Adv. Mater.,* 2013, **25**, 2969.

TOC

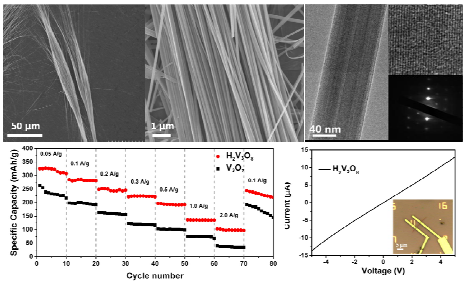

Text

In situ transport measurement of single nanowire demonstrates that the $H_2V_3O_8$ nanowire possesses good electrical transport properties.